Influence of the free-energy functional form on simulated morphology of spinodally decomposing blends

Aleksij Aksimentiev[1] and Robert Hołyst[2,3]
[1]*Material Science Laboratory, R&D Center, Mitsui Chemicals, Inc., 580-32 Nagaura, Sodegaura-City, Chiba 299-0265, Japan*
[2]*Institute of Physical Chemistry PAS College of Science, Kasprzaka 44/52, 01-224 Warsaw, Poland*
[3]*Laboratoire de Physique, Ecole Normale Superieure de Lyon, Allee d'Italie 46, 69364 Lyon, Cedex 07, France*
(Received 17 April 2000)

The spinodal decomposition of a binary mixture has been studied within several mesoscopic models. It has been found that the form of the equilibrium free energy has a crucial effect on the morphological development in asymmetric blends. We have shown that the principal quantity that determines the topology of the interface (and type of morphology) is the equilibrium minority phase volume fraction, while the transition from bicontinuous to droplet morphology can be treated as a percolation. The concentration dependence of the square gradient coefficient attributed for the Flory-Huggins–de Gennes free energy has no significant influences on the average domain growth, but can be distinguished experimentally from its constant-coefficient alternative by measuring the maximum wave vector of the scattering intensity as a function of the minority phase volume fraction for spinodally decomposing asymmetric blends. The concentration dependence of the Onsager coefficient has the weak, systematic effect of slowing down the morphological development. The local shape of the interface is not affected considerably by the concentration dependence of the square gradient and Onsager coefficient.

PACS number(s): 64.75.+g, 64.60.−i

I. INTRODUCTION

A homogeneous A/B binary mixture after a rapid change of external conditions (quench) can be driven into a thermodynamically unstable state that will cause a phase separation process. By a rapid enhancement of concentration fluctuations domains rich in A or B components will be formed shortly after the quench. These domains will grow with time, changing the length scale of the phase separation from the microscopic molecular scale of the very early times to the macroscopic scale of the final stages of this process, comparable with the system size. Therefore, time-dependent mesoscopic models that cover the most interesting intermediate regime of the growth have become a convenient framework for modeling these phenomena. Governed by the same general principles, time-dependent mesoscopic models were successfully used to study the decomposition kinetics in both simple and complex mixtures [1–3]. However, the final form of the Cahn-Hilliard-Cook equation, which has to be solved numerically, is very dependent on the model coarse-grained free-energy functional and Onsager coefficient specifically chosen for a given system. However, even for the same system, the final dynamic equation may take different forms [4–9] depending on the simplifying assumptions made by authors about the free-energy functional and Onsager coefficient. At the same time, these equations should describe kinetics of essentially the same systems. The main purpose of this paper is to answer the following question: ''What influence do model assumptions about the coarse-grained free-energy and Onsager coefficient have on the *morphology* development during the simulated phase separation process?''

Let us consider a dynamically symmetric binary mixture described by the scalar order parameter field $\phi(\mathbf{r})$, which is the local volume fraction of component A at point $\mathbf{r}$. The order parameter $\phi(\mathbf{r})$ should satisfy the local conservation law, which can be written as a continuity equation [10]

$$\frac{\partial \phi(\mathbf{r},t)}{\partial t} = -\nabla \mathbf{J}_A(\mathbf{r}) + \eta(\mathbf{r},t), \tag{1}$$

where $\nabla \mathbf{J}_A(\mathbf{r})$ is the local flux of the A component, and the stochastic term $\eta(\mathbf{r},t)$ represents the thermal noise [1–3]. Let us assume that the molecular transport is governed only by the differences in the chemical potential (diffusion), and neglect possible order parameter transport by the hydrodynamic flow [3,11,12]. Then one can postulate a linear relationship between the local current and the gradient of the local chemical potential difference $\mu(\mathbf{r})$ [13,14] as

$$\mathbf{J}(\mathbf{r}) = -\int \frac{\Lambda(\mathbf{r}-\mathbf{r}')}{k_B T} \nabla' \mu(\mathbf{r}') d\mathbf{r}. \tag{2}$$

Here $\Lambda(\mathbf{r}-\mathbf{r}')$ is the Onsager coefficient that specifies the transport properties of the considered system at a certain time and length scale, and which is nonlocal in general. The local chemical potential difference $\mu(\mathbf{r})$ can be found in a standard way as a functional derivative of the coarse-grained free-energy functional $F[\phi]$:

$$\mu(\mathbf{r}) = \frac{\delta F[\phi]}{\delta \phi(\mathbf{r})}. \tag{3}$$

Finally, the noise term in Eq. (1) should satisfy the appropriative fluctuation-dissipation relation [3]. In this way, all information about specific properties of the system enters into the dynamic equation (1) via the free-energy functional and Onsager coefficient.

The simplest free-energy functional that describes an inhomogeneous mixture can be written in the form

$$F[\phi(\mathbf{r})]=k_BT\int d^3r[f(\phi(\mathbf{r}))+K(\nabla\phi(\mathbf{r}))^2], \qquad (4)$$

where $f(\mathbf{r})$ is the homogeneous (bulk) free energy of the mixing. The square gradient term in Eq. (4) measures the free-energy cost of the inhomogeneities (interface), and the coefficient K is often regarded as the ''range'' of the interactions [1]. In the case of a symmetric homopolymer mixture, the equilibrium free energy can be written in the Flory-Huggins (FH) form [15]

$$f(\phi)=\frac{1}{N}\{\phi\ln(\phi)+(1-\phi)\ln(1-\phi)\}+\chi\phi(1-\phi), \qquad (5)$$

where N is the polymerization index and χ is the FH interaction parameter. This expression was originally derived to describe the system of polymer chains on a lattice, but can also be used in course-grained models. In this case, the Flory-Huggins interaction parameter measures an effective, relative affinity between A and B components, averaged over some mesoscopic length scale, and can be determined phenomenologically from experiments. The only specific polymer feature of the FH free energy is its dependence on the polymerization index N, which simply refers to the fact that N monomers form one macromolecule. Therefore, the coarse-grained free energy of mixing for a simple binary mixture must be given by the same expression, [Eq. (5)], but with $N=1$. On the other hand, near the critical point, the free-energy can be written in the standard Landau-Ginzburg (LG) form with its homogeneous part:

$$f(\phi(\mathbf{r}))=-\tfrac{1}{2}r\tilde{\phi}(\mathbf{r})^2+\tfrac{1}{4}u\tilde{\phi}(\mathbf{r})^4. \qquad (6)$$

Here r and u are positive phenomenological constants [4], and $\tilde{\phi}=\phi-\phi_c$ (ϕ_c is the critical value of the order parameter). It was speculated [16] that the specific form of the FH free energy may be responsible for some experimentally observable nonuniversalities of the polymer blend phase separation, while none of those were observed in computer simulations with the LG free energy. Since the LG free energy can be obtained by expanding Eq. (5) in ϕ around the critical concentration, no significant differences between those two models appear within the critical region. Here we shall show that even far from the critical region the LG free energy with correctly chosen parameters leads to quantitatively the same phase-separated morphology, i.e., the average domain size and the interface topology, if it is used instead of the FH expression in the computer simulations.

The square-gradient term in Eq. (4) can be derived from the Landau-type free-energy functional expansion by identifying that term with the lowest-order inhomogeneous correction. This formalism implies that an expansion of the inhomogeneous system free energy above that of the reference homogeneous system was made [17], and, therefore, coefficients of this expansions are constants (evaluated for the reference uniform system). A more detailed form of K can be surmised from the shape of the equilibrium correlation function that in the case of the polymer blend (within the random phase approximation) is [15]

$$\left(\frac{\delta^2F}{\delta\phi^2}\right)_{\mathbf{q}}\equiv S^{-1}=\frac{1}{N\phi_0D(q^2R_g^2)}+\frac{1}{N(1-\phi_0)D(q^2R_g^2)}-2\chi, \qquad (7)$$

where R_g is the polymer chain radius of gyration, $D(x)$ is the Debye function, ϕ_0 is the average volume fraction of the A component, and the incompressibility constraint has been imposed. Expanding the Debye function in the limit of small q as

$$D(x)=(2/x)(1-(1-e^{-x})/x)\approx 1-x/3, \qquad (8)$$

where $x=(qR_g)^2$, the following form of K can be found [18]:

$$K=\frac{1}{36}\frac{\sigma^2}{\phi_0(1-\phi_0)}. \qquad (9)$$

Here σ is the statistical Kuhn segment length [15], such that $R_g=\sqrt{N}\sigma/\sqrt{6}$. The truncation of the infinite Landau-type expansion at the lowest order term is justified when the order parameter gradients are small, which requires a smooth variation of the order parameter through the interface. In the case of polymer mixtures this truncation can be made when the interface width is larger than the polymer chain radius of gyration ($q^2R_g^2\ll 1$). The higher order corrections for Eq. (4) can be derived in a systematic way [17,18].

An alternative way to find the expression for K is to assume that the same form of the structure factor [Eq. (7)] will also be valid locally for the inhomogeneous system, if the average volume fraction ϕ_0 in Eq. (7) is replaced by its local values $\phi(\mathbf{r})$. Guided by this assumption one can allow the coefficient at the gradient term to be dependent on the local volume fractions, and write K as

$$K(\phi)=\frac{1}{36}\frac{\sigma^2}{\phi(\mathbf{r})[1-\phi(\mathbf{r})]}. \qquad (10)$$

Is was argued [7] that this concentration dependence of K describes the loss of the conformation entropy related to some specific chain conformations at the interface. The free-energy functional in the form of Eq. (4), with the FH bulk free energy and a nonconstant square gradient coefficient [Eq. (10)], was postulated by de Gennes [13], and has since, been widely used by other [10,14,5,7] to model the phase separation phenomena in polymer mixtures. It must been stressed that no rigorous derivation of the above expression can be made from the standpoint of the traditional Landau-type analysis [17]. The first derivation of the Flory-Huggins–de Gennes free-energy was made by Tang and Freed [17] within the framework of the density functional theory. Despite the considerable clarification of the theoretical aspects of this problem, it is still not known which functional with a constant or nonconstant square-gradient coefficient better describes behaviors of real systems. In this paper we compare morphological evolutions simulated for both free-energy functionals.

The most frequently used expression for the Onsager coefficient for a simple binary mixture reads

$$\Lambda(\mathbf{r}-\mathbf{r}')=M\delta(\mathbf{r}-\mathbf{r}'), \qquad (11)$$

where M is a phenomenological mobility. For a polymer blend, the form of the Onsager coefficient depends on the scale on which the phase separation is considered. If the minimal length scale detectable in the simulations (mesh size) is larger than the radius of gyration of a polymer coil, then the nonlocal Onsager coefficient [10,14] can be approximated as

$$\Lambda(\mathbf{r}-\mathbf{r}')=DN\phi(1-\phi)\,\delta(\mathbf{r}-\mathbf{r}'), \tag{12}$$

where D is the self-diffusion constant of a polymer chain. In the last expression, the concentration dependence of the Onsager coefficient originates from the zero total current divergence constraint that must be satisfied for any incompressible system [13]. Therefore, the Onsager coefficient for any simple mixtures that can be considered incompressible must also be concentration dependent. However, this dependence of Λ is often disregarded in the computer simulations [4,5,19]. We shall show below what influence this simplification has on the phase separation kinetics.

In Sec. II we discuss the time evolutions of several characteristic measures of the phase separated morphology that have been simulated within six different mesoscopic models of the same binary mixture. The influence of the equilibrium free-energy form $f(\phi)$, the concentration dependence of the square gradient coefficient, and the concentration dependence of the Onsager coefficient will be investigated. Results are summarized in Sec. III.

II. RESULTS AND DISCUSSION

A symmetric binary homopolymer mixture ($N_A=N_B=N$ and $\sigma_A=\sigma_B=\sigma$) has been used as a model system for all further investigations. Since the phase diagram of this system is symmetric, only the left part ($\phi_0\leqslant 0.5$) has been considered. Dynamic equation (1) has been solved numerically on the cubic 96^3 lattice by using the explicit Euler scheme. No finite size effects have been observed within the time intervals studied. The following rescaled variables have been used:

$$\mathbf{x}=\frac{(\chi-\chi_s)^{1/2}}{\sigma}\mathbf{r}, \tag{13}$$

$$\tau=\frac{D(\chi-\chi_s)^2}{\chi_s\sigma^2}t. \tag{14}$$

In the above expressions, χ is the Flory-Huggins parameter, and $\chi_s=1/(2N\phi_0(1-\phi_0))$ and $\chi_{cr}=2/N$ are the values of χ at the spinodal and critical points, respectively. In accordance to the previous studies [5,6], all phenomena will be described in the experimental rescaled variables [16]. The new rescaled time τ_e and distance $\mathbf{r}_e$ are

$$\tau_e=18\phi_0(1-\phi_0)\,\tau, \tag{15}$$

$$\mathbf{r}_e=\sqrt{18\phi_0(1-\phi_0)}\,\mathbf{x}. \tag{16}$$

The numerical prefactors in Eqs. (15) and (16) originate in the linearized theory of the critical quench [5]. In all figures the subscript e in τ_e will be omitted.

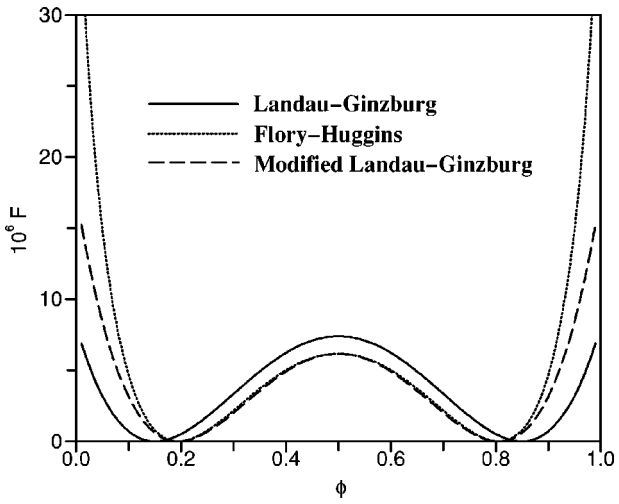

FIG. 1. The homogeneous free energies computed at $T=25°C$ by using the Flory-Huggins (FH) expression [Eq. (18)], and the Landau-Ginzburg expressions Eqs. (19) (LG) and (20) (LG_M).

In order to make comparison between our simulation and previous simulations, we took the input parameters that correspond to the previously studied polybutadienes system [20,16,7]. We shall assign different quench conditions to the temperature changes of the polybutadiene-deuterated polybutadien system by using the experimental dependence [20]

$$\chi=0.326/T-0.00023. \tag{17}$$

The critical temperature measured for this system is about 62 °C ($\chi_{cr}=7.43\times10^{-4}$). More details about the simulation procedure can be found in Ref. [9].

A. Landau-Ginzburg and Flory-Huggins homogeneous free-energies

The Flory-Huggins free energy in the rescaled variables [Eq. (14)] reads

$$F_{FH}=\tfrac{1}{2}[\phi\log(\phi)+(1-\phi)\log(1-\phi)]\chi_{cr}+\phi(1-\phi)\chi. \tag{18}$$

The Landau-Ginzburg free energy can be obtained from Eq. (18) by expanding it in powers of $\phi-\phi_c$ ($\phi_c=0.5$) and keeping all terms up to the fourth order:

$$F_{LG}=\tfrac{2}{3}(\phi-0.5)^4\chi_{cr}+(\chi_{cr}-\chi)(\phi-0.5)^2. \tag{19}$$

There are several important differences between the FH [Eq. (18)] and LG [Eq. (19)] expressions for the free energy (illustrated in Fig. 1). First, the equilibrium volume fractions of the component A in the B component rich phase, ϕ_1^{eq}, is always lower for the free energy given by Eq. (19). Consequently, the equilibrium volume fraction of the minority phase, f_m^{eq} (the phase rich in the A component), determined by the lever rule from the phase diagram is always higher for the LG expression. Please note that, only for a symmetric mixture, $f_m=f_m(\tau)=\phi_0=0.5$. For any asymmetric composition ($\phi_0\neq0.5$) the volume fraction of the minority phase, f_m, decreases with time, approaching its equilibrium value f_m^{eq}. It will be shown below that this feature significantly modifies the morphology development in asymmetric (ϕ_0

$\neq 0.5$) blends. Second, the difference between the minimum $[F(\phi_1^{eq})]$ and maximum $[F(1/2)]$ values of the free-energy density is larger for the LG expression (19), if compared to the FH expression. Third, the shapes of the tails at $\phi \to 0$ and $\phi \to 1$ are essentially different. The unphysical values of $\phi < 0$ and $\phi > 1$ are automatically forbidden for the FH free-energy expression, while for the LG one they are formally allowed. The first two disparities can be corrected if, instead of expression (19) the modified LG homogeneous free energy (LG_M) will be postulated as

$$F_{LG_M} = [\alpha(\chi)^{\frac{2}{3}}(\phi - 0.5)^4 \chi_{cr} + (\chi_{cr} - \chi)(\phi - 0.5)^2]\beta(\chi). \tag{20}$$

The two constants α and β have to be chosen in such a way that the equilibrium volume fraction of the A component in the B phase, ϕ_1^{eq}, and the free-energy difference $F_{LG_M}(\phi_1^{eq}) - F_{LG_M}(1/2)$, are exactly the same as those for the FH free energy at a given χ. The FH, LG, and LG_M free energies, are plotted in Fig. 1 for $\chi = 8.64 \times 10^{-4}$ ($T = 25\,^{\circ}\mathrm{C}$).

The FH, LG, and LG_M bulk free energies, combined with the square-gradient term in the form of Eq. (9) were substituted into the dynamic equation (1) together with the constant Onsager coefficient (11). The sequence of the order parameter configurations has been analyzed by computing the pair correlation function, structure factor, and several other morphological measures [9]. The average domain size has been determined by locating either the first zero in the pair correlation function, R_0, or the maximum of the structure factor, q_m. The interface topology has been characterized by computing the Euler characteristic [9,21,22]. The Euler characteristic describes the connectivity of the domains and is related to the other topological measure, the genus g, as $\chi_{Euler} = 2(1-g)$. The genus has a simple geometrical meaning: it counts the number of holes in a closed surface. Also, for a closed surface, the Gauss-Bonnet theorem relates the Euler characteristic to the surface integral from the local Gaussian curvatures, $K_G(\mathbf{r})$:

$$\chi_{Euler} = \frac{1}{2\pi} \int_S K_G(\mathbf{r}) dS. \tag{21}$$

The Euler characteristic is an additive measure [22]. Therefore, the interconnected bicontinuous morphology is characterized by the large and negative Euler characteristic, while for the droplet-matrix morphology it is large and positive [23]. The algorithm used to calculate the Euler characteristic was discussed in Refs. [9] and [21].

The domain growth simulated for the FH, LG, and LG_M bulk free energies is shown in Figs. 2(a) and 2(b). There are minor deviations in the average domain growth regarding to the form of the homogeneous free-energy in both symmetric [Fig. 2(a)] and asymmetric [Fig. 2(b)] blends. Also, the Euler characteristic density in the symmetric cases does not depend much on the form of the homogeneous free energy, [Fig. 3(a)]. However, for asymmetric blends the topology of the simulated interface depends significantly on the model equilibrium free energy. The interface simulated with the unmodified LG free energy, [Eq. (19)], is more interconnected, if compared to the interfaces simulated within the other models at the same conditions [Figs. 3(a) and 3(b)]. At some special quench conditions $\chi = 9.02 \times 10^{-4}$ and $\phi_0 = 0.35$ [Fig. 3(b)], the simulated morphologies differ even qualitatively: the droplet-matrix morphology is observed for the FH or modified LG free-energy expression, but for the unmodified LG expression the simulated morphology is bicontinuous. This discrepancy is directly related to the larger equilibrium minority phase volume dictated by the unmodified LG free-energy form [Eq. (19)]. At the same time, if the minima of the LG and FH free energies coincides, then no significant differences between the Euler characteristic evolutions are observed. The tail shape of the free energy slightly modifies the local volume fraction probability distributions. That in turn affects the way the phase volumes approach their equilibrium limits (Fig. 4). Due to that fact, the FH and LG_M curves deviate from each other at the beginning times of the simulation.

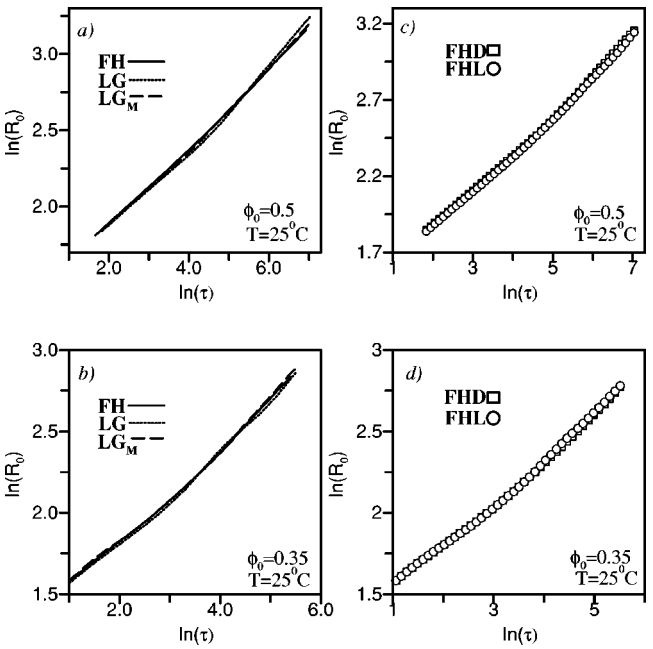

FIG. 2. The growth of the domains estimated from the first zeros, R_0, in the pair correlation functions. The following models have been compared: (a) and (b) Models with the homogeneous Flory-Huggins (FH), Landau-Ginzburg (LG), or modified Landau-Ginzburg (LG_M) free-energies, constant square gradient and Onsager coefficients. (c) and (d) Flory-Huggins–de Gennes (FHD) and Flory-Huggins constant square-gradient coefficient (FHL) models with nonconstant Onsager coefficients.

B. Flory-Huggins–de Gennes and Flory-Huggins Landau-type inhomogeneous free-energies

The Flory-Huggins–de Gennes (FHD) free energy is constructed by combining the equilibrium Flory-Huggins free energy [Eq. (18)], with the square-gradient term in the form of Eq. (10). Our aim is to detect the influences that the nonconstant coefficient at the square-gradient term has on the morphology development during spinodal decomposition. In order to do that, we construct a slightly different inhomogeneous free energy, which is referred to here as the Flory-Huggins-Landau- (FHL) type free energy, by combining the FH expression [Eq. (18)], with the square-gradient term in

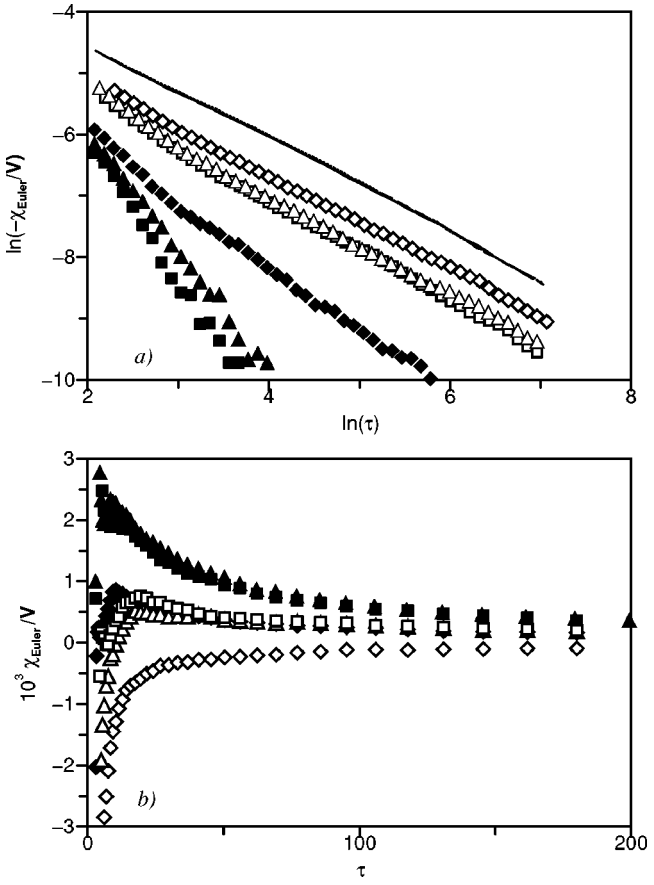

FIG. 3. The influence of the homogeneous free-energy form on the time evolution of the Euler characteristic density. The different values of the equilibrium phase volumes derived from the form of the equilibrium free energy (Fig. 1) significantly modifies topological properties of the interface. The symbols correspond to the considered models as follows: for $\phi_0=0.5$, the FH free energy corresponds to a solid line, LG to a dotted line, and LG_M to a long-dashed line. For $\phi_0\neq 0.5$, FH is represented by triangles, LG by diamonds and LG_M by squares. The quench conditions are (a) $\phi_0=0.5$ at $T=25\,^\circ$C (lines), $\phi_0=0.4$ at $T=25\,^\circ$C (empty symbols), and $\phi_0=0.4$ at $T=40\,^\circ$C (filled symbols); and (b) $\phi_0=0.35$ at $T=15\,^\circ$C (empty symbols) and $\phi_0=0.35$ at $T=25\,^\circ$C (filled symbols).

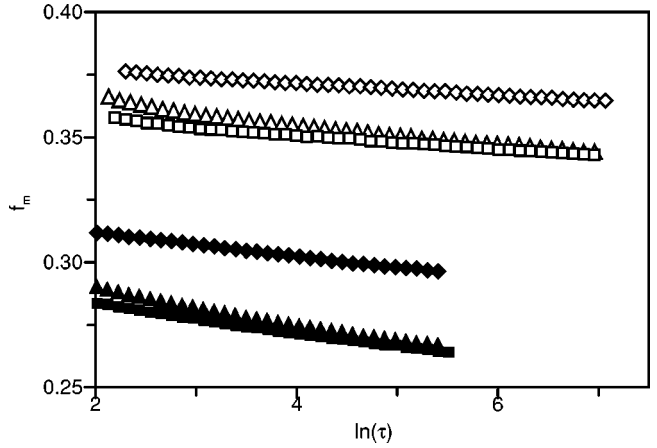

FIG. 4. The influence of the homogeneous free-energy form on the time evolution of the minority phase volume fraction, f_m. The tail shape of the free-energy (Fig. 1) modifies the way the phase volumes approach their equilibrium limits. The symbols correspond to the considered model as follows: FH is represented by triangles, LG by diamonds, and LG_M by squares. The quench conditions are $\phi_0=0.4$ at $T=25\,^\circ$C (empty symbols) and $\phi_0=0.25$ at $T=25\,^\circ$C (filled symbols).

form Eq. (9). Both functionals have been substituted into the dynamic equation (1) together with the concentration-dependent Onsager coefficient [Eq. (12)].

The domain growth simulated within the FHD and FHL models is shown in Fig. 2 for symmetric [Fig. 2(c)] and asymmetric [Fig. 2(d)] blends. There are no significant deviations between them. Also, the Euler characteristic density evolution, [Fig. 5(a)], is insensitive to the concentration dependence of the square-gradient term. However, the time evolution of the average mean curvature defined as

$$\langle H\rangle=\frac{\int H(\mathbf{r})dS}{S}, \tag{22}$$

where S is the total interface area, depends on the free-energy form used in the simulations [Fig. 5(b)]. For symmetric blends, $\langle H\rangle$ fluctuates around zero due to the symmetry of the phase volume fractions. In the slightly asymmetric blends ($\phi_0=0.4$), the average mean curvature changes its sign with time, which reflects a transformation [9] from the percolated cluster morphology of $\langle H\rangle<0$ to the ''interconnected passage'' structure of $\langle H\rangle>0$ (the mean curvature of a single A-type droplet is defined as negative). Our observation is that within the FHD model this transformation occurs more rapidly. Also, in the case of the droplet-matrix morphology ($\phi_0=0.35,\chi=9.02\times10^{-4}$), the absolute value of the average mean curvature is smaller for the FHD model.

One may assume that the difference in the average mean curvature behaviors originates in some local interfacial properties described by the concentration dependence of K within the FHD model, but ignored for the FHL model. However, as will be shown in Sec. II C (Fig. 11), the local properties of the interface are insensitive to the form of the dynamic equation. The only factor that affects the average mean curvature evolution is the change of the phase volume with time. In Fig. 6(a) the time dependence of the minority phase volume, f_m, simulated within both models is shown for $\phi_0=0.4$ and $\chi=8.64\times10^{-4}$. When the FHD model predicts a more rapid decrease of the minority phase volume fraction, the topology of the interface must be the same as for the FHL model [Fig. 5(a)]. This requires a significant modification of the total interface shape, which is quantitatively indicated by the different values of the average mean curvature.

It has been argued [24,7] that the concentration dependence of the square-gradient term reflects some entropic contributions related to specific configurations of the polymer chains at the interface. In this case, the entropic barrier associated with the transport of the polymer chains across the interface must slow down the phase separation process. A dynamic model in which such effects are taken into account must result in a slower morphology development. In contrast, very similar time evolutions of the average domain size and the Euler characteristic of the phase-separated structures have been found, regardless of the concentration dependence

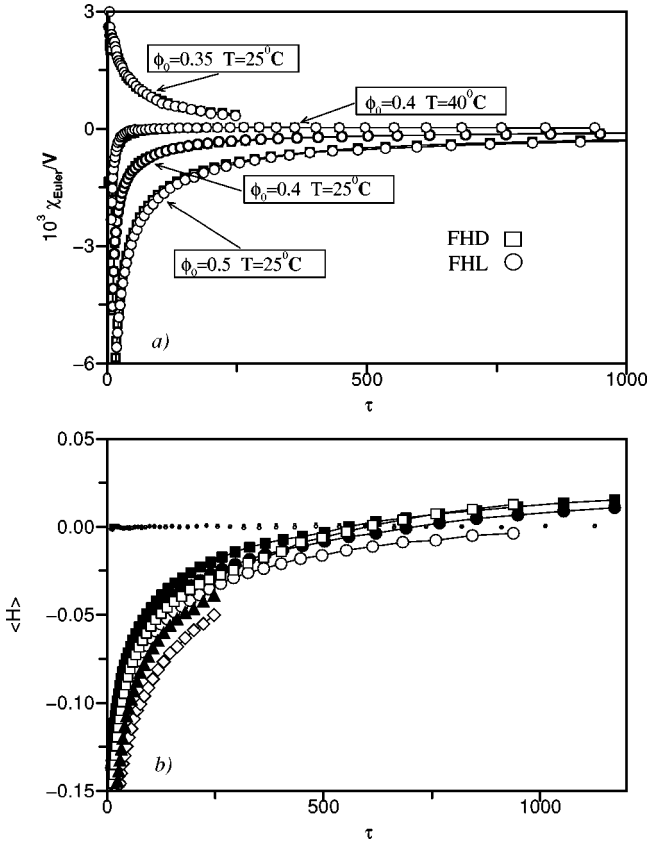

FIG. 5. The influence of the concentration dependence of the square-gradient coefficient on the time evolution of the Euler characteristic density (a) and the average mean curvature (b). The data obtained within the FHD model are represented by squares, and these from the FHL model by circles. The quench conditions are (a) from bottom to top, $\phi_0=0.5$ at $T=25°$, $\phi_0=0.4$ at $T=25\,°\mathrm{C}$, $\phi_0=0.4$ at $T=40\,°\mathrm{C}$, and $\phi_0=0.35$ at $T=25\,°\mathrm{C}$; and (b) $\phi_0=0.5$ at $T=25\,°\mathrm{C}$ (small symbols), $\phi_0=0.4$ at $T=25\,°\mathrm{C}$ (filled symbols), $\phi_0=0.4$ at $T=40\,°\mathrm{C}$ (empty symbols), and $\phi_0=0.35$ at $T=15\,°\mathrm{C}$ [FHD (filled triangles) and FHL ($\diamond$)].

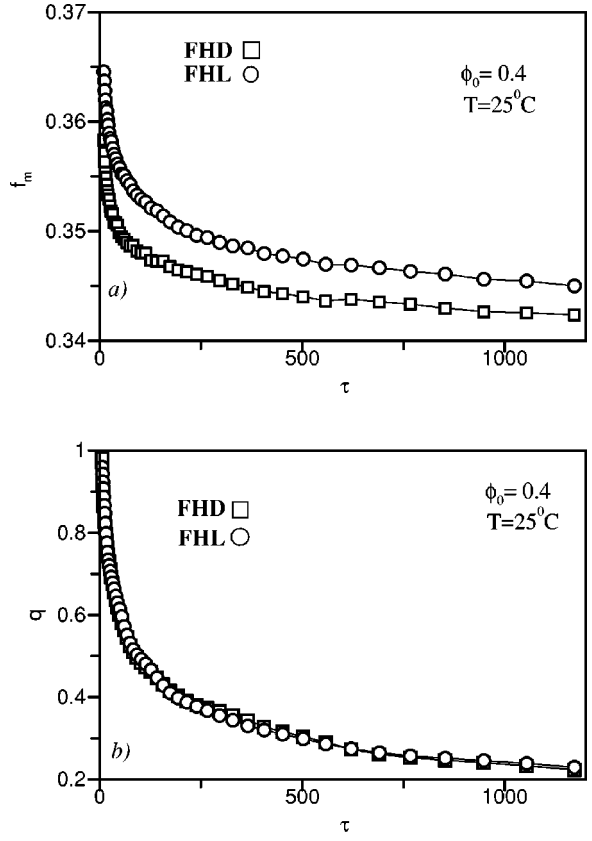

FIG. 6. The influence of the concentration dependence of the square-gradient coefficient on the time evolution of the minority phase volume fraction (a), and the peak position in the scattering intensity (b). The data from the FHD model are represented by squares, and these from the FHL by circles.

of K. Even more, the volume fraction of the minority phase approaches its equilibrium value faster within the FHD model [Fig. 6(a)], which can be explained by the larger (on average) contribution from the square-gradient term in the concentration-dependent case. Thus we conclude that no slowing down due to the concentration dependence of K has been observed in the simulations. This may also indicate that in order to investigate such a specific polymer feature of the phase separation kinetics the model must operate at much smaller length scales.

The absolute magnitude of the constant square-gradient coefficient measures the free-energy cost of the interface. For a model with a smaller K a larger amount of the interface can be formed. Therefore the resulting morphology development is slower. In Fig. 7 the time evolution of several morphological measures simulated for the FHL models with $K=\gamma K_0$ for $\gamma=1(\bigcirc),0.5(\bigtriangledown),1.5(\bigtriangleup)$ $(K_0=\frac{1}{36}\sigma^2/[\phi_0(1-\phi_0)])$ and for the FHD model (squares) are shown. At the same rescaled time unit, the average domain size is smaller for the model with the smaller K [Fig. 7(a)], but the interface is more interconnected since the absolute value of the Euler characteristic is larger [Fig. 7(b)]. The dimensionless quantity that characterizes the shape of the bicontinuous interface is the homogeneity index I_H

$$I_H=\left[-\frac{S^3}{2\pi\chi_{Euler}V^2}\right]^{1/2}. \tag{23}$$

This combines the area to volume ration with the Euler characteristic of the hyperbolic surface [25]. The time evolutions of the homogeneity index are shown in Fig. 7(c). There are no systematic deviations of the homogeneity index time evolutions regarding the change of K. In contrast, the time dependence of the minority phase volume fraction, [Fig. 7(d)] is drastically affected by the K decrease. For the smallest square gradient coefficient, the domain volume fractions are already at equilibrium very shortly after the quench. That affects crucially the process of the droplet morphology formation [26]. The droplets are formed earlier with the smaller average size and larger droplet number density if compared to the standard model (the FHL model).

Unfortunately, it is still not possible to measure the average mean curvature for a real polymer system [27,28] within the accuracy that is required to make an experimental judgment about the proper free-energy form. Nevertheless, an experimental investigation of this problem is possible, since a precise measurement of the phase volume fractions can made by analyzing TEM or scanning electron microscopy micrographs [29]. One can simply measure the time interval that is required to achieve a certain fracture of the minority phase volume during the spinodal decomposition, and compare it with the simulation results. For example, a time inter-

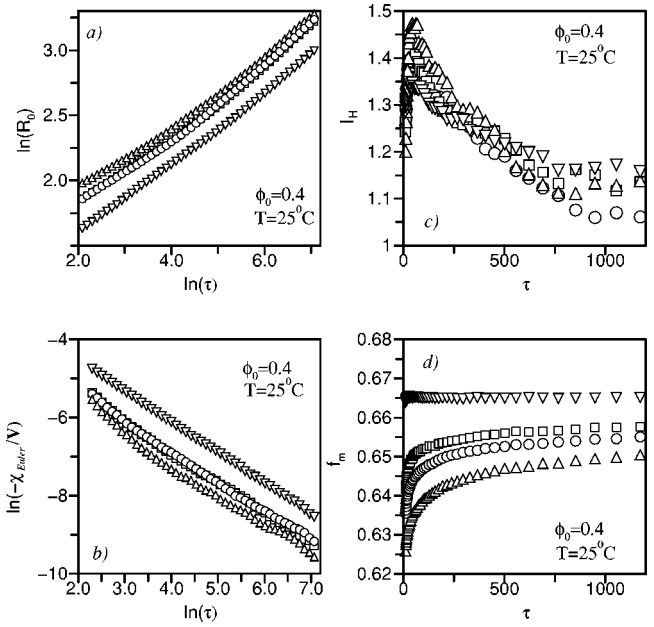

FIG. 7. The influence of the magnitude of the constant square-gradient coefficient on the morphology of the phase separation. The average domain size (a), the Euler characteristics density (b), the homogeneity index $I_H=[-S^3/2\pi\chi_{euler}V^2]^{1/2}$ (c), and the minority phase volume fraction (d) are plotted for the FHD model (squares), and for the FHL models with the standard, [Eq. (9)] (○) constant square-gradient coefficients two times smaller (▽) and 1.5 times larger (△).

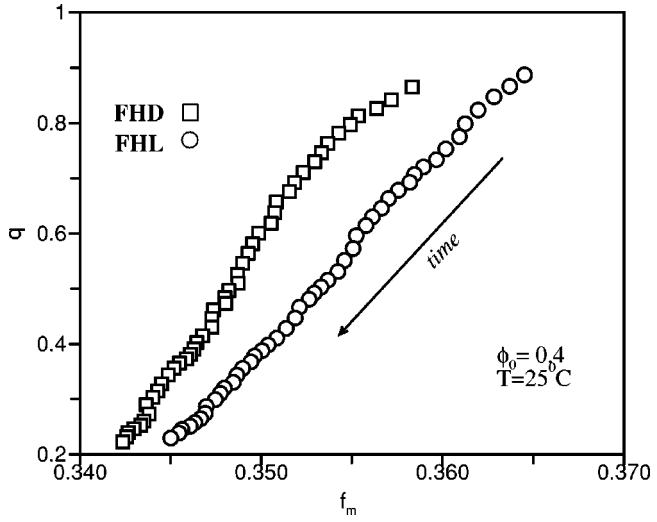

FIG. 8. The peak wave-vector position in the scattering intensity as a function of the minority phase volume fraction simulated within the FHD (squares) and FHL (circles) models.

val more than three times longer is required to achieve the volume fraction of minority phase $f_m=0.345$ within the FHL model if compared to the time predicted for the FHD model [Fig. 6(a)]. However, this experimental scheme requires precise measurements of the self-diffusion constant and the Flory-Huggins interaction parameter in order to calculate the absolute time from Eq. (14). However, since both models predict very similar time dependences of the peak wave-vector position in the scattering intensity, [Fig. 6(b)], they can be used as a measure of the rescaled time. The peak wave vector as a function of the minority phase volume fraction is plotted in Fig. 8 for both models. There are considerable differences between the simulated dependences. By measuring a similar experimental dependence the relevance of the FHD and FHL models for a description of the real system phase separation can be determined. The only parameters needed to compare simulations with experimental results are the average blend composition ϕ_0 and the temperature dependence of the Flory-Huggins parameter. Both components of the experimental blend must have similar polymerization indices and Kuhn segment lengths, a slightly asymmetric average composition ($\phi_0=0.4$), and good contrast on scanning electron microscope (SEM) or TEM micrographs.

C. Concentration dependence of the Onsager coefficient

In order to detect the influences that the concentration dependence of the Onsager coefficient has on the morphology development, the FHD and FHL models have both been simulated with constant [Eq. (11)] and concentration dependent [Eq. (12)] Onsager coefficients. The fluctuation-dissipation theorem that defines the way the noise term in Eq. (1) is generated was consequently modified [9,30]. To generate the noise for concentration dependent Onsager coefficient [Eq. (12)], we introduce the additional vector white noise $\vec{\xi}$ with the Gaussian components, which satisfies the following relation:

$$\langle \xi_i(\mathbf{x},\tau)\xi_j(\mathbf{x}',\tau')\rangle = \frac{\phi(\mathbf{x})(1-\phi(\mathbf{x}))}{\phi_0(1-\phi_0)}\delta_{i,j}\delta(\mathbf{x}-\mathbf{x}')\delta(\tau-\tau'). \tag{24}$$

If we now relate the rescaled noise variable $\zeta(\mathbf{x},\tau) \equiv \epsilon^{-1/2}\eta(\mathbf{r},t)$ to ξ as

$$\zeta(\mathbf{x},\tau)=\nabla\vec{\xi}(\mathbf{x},\tau), \tag{25}$$

the fluctuation-dissipation theorem (FDT) will be satisfied. The white noise components are generated from the Gaussian distribution with the variance $[\phi(\mathbf{x})(1-\phi(\mathbf{x}))]/[\phi_0(1-\phi_0)]$ independently at each lattice site. The noise intensity $\epsilon=\sqrt{(\chi-\chi_s)}$.

The simulated domain growth for the symmetric and asymmetric blends is shown in Figs. 9(a) and 9(b), respectively. The curves simulated with the constant Onsager coefficient deviate systematically from those simulated with the concentration dependent coefficient. In the former case, the domain always has a larger (up to 10% at late times) average size. This fact can be explained qualitatively if one considers a discretized version of the dynamic equation. For the same order parameter configuration, within one time step of the iteration procedure, the ratio of the one-step local order parameter change computed with the concentration dependent Λ to that computed with the constant Λ is proportional to $\phi(\mathbf{r})(1-\phi(\mathbf{r}))/[\phi_0(1-\phi_0)]$. Therefore, within the one time step, the average magnitude of the order parameter change is larger for the model where the constant Onsager coefficient is used. This results in the faster phase separation dynamics and the larger average domain size for the constant Onsager coefficient scheme. However, the influence of the concentration dependence of Λ cannot be reduced to a

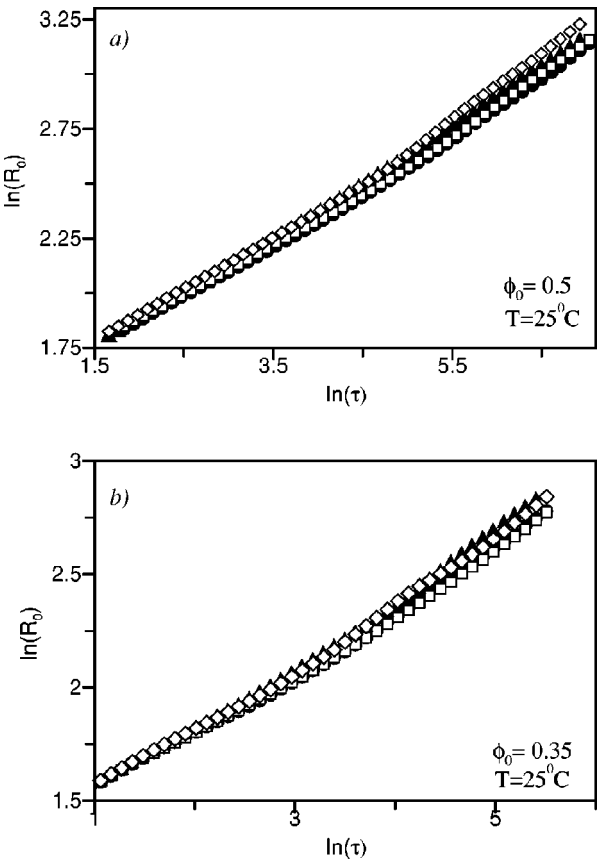

FIG. 9. The domain growth estimated from the first zeros, R_0, in the pair correlation functions compared for models with constant and concentration dependent Onsager coefficients. The following four models have been considered: the FHL model with the constant (triangles) and concentration dependent (circles) Onsager coefficients; and the FHD model with the constant ($\diamond$) and concentration dependent (squares) Onsager coefficients.

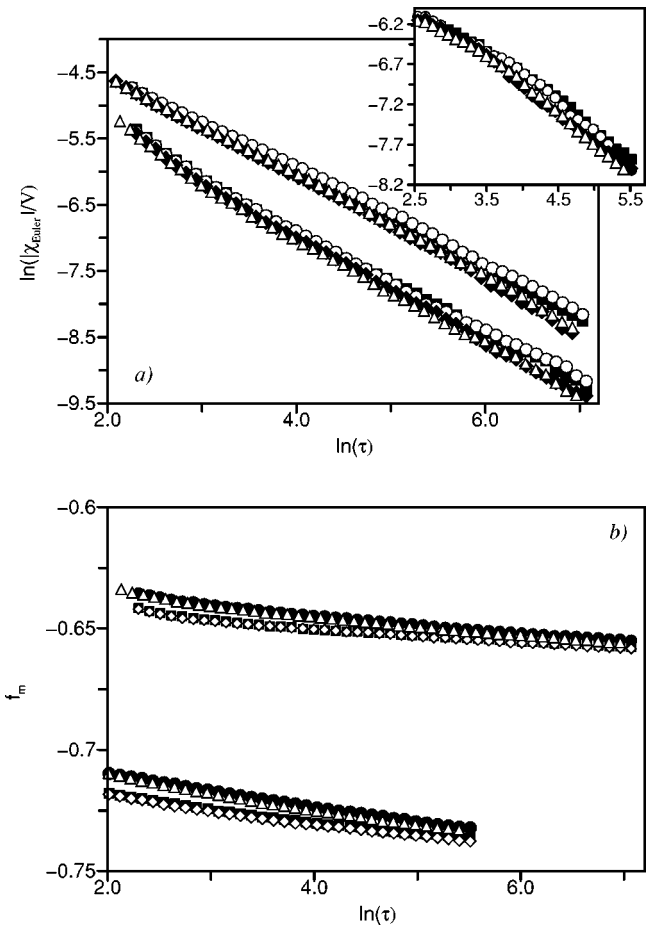

FIG. 10. The influence of the concentration dependence of the Onsager coefficient on the time evolution of the Euler characteristic density (a), and the minority phase volume fraction (b). The symbols have the same meaning as in Fig. 9 (the filling of the symbols has been changed). The quench conditions shown are (a) $\phi_0=0.5$ at $T=25\,^{\circ}\mathrm{C}$ (four upper lines), $\phi_0=0.4$ at $T=25\,^{\circ}\mathrm{C}$ (four lower lines), and $\phi_0=0.35$ at $T=25\,^{\circ}\mathrm{C}$ (inset); and (b) $\phi_0=0.4$ at $T=25\,^{\circ}\mathrm{C}$ (four upper lines) and $\phi_0=0.35$ at $T=25\,^{\circ}\mathrm{C}$ (four lower lines).

simple rescaling of the time unit, since it could also slightly modify the slope of the domain growth [Fig. 9(a)].

The interface topology, that is characterized by the Euler characteristic density [Fig. 10(a)], is affected by the form of the Onsager coefficient in a similar manner. For the constant Onsager coefficient, the connectivity of the bicontinuous interface is smaller if compared to the morphology simulated for the concentration dependent case. The same dependence also holds in the case of the droplet morphology, $\phi_0=0.35,\chi=8.64$ [inset in Fig. 10(a)]. In this case the Euler characteristic density is exactly twice the droplet number density. We have found that for a constant Onsager coefficient a smaller number of droplets with a larger average size is observed in comparison to simulations performed with the concentration dependent Λ.

The temporal evolution of the minority domain volume fraction is not very sensitive to the form of the Onsager coefficient [Fig. 10(b)]. There is a small systematic decrease of f_m in the case of the constant Onsager coefficient. However, this effect is much smaller in comparison to the similar effect of the minority phase volume change when, instead of the constant, the concentration dependent square gradient coefficient $K(\phi)$ in the free-energy functional is used. The time evolution of the average mean curvature depends both on the form of Λ and K. In the case of the bicontinuous asymmetric blends, the concentration dependence of both factors speed up the zero average mean curvature transition, while in the case of droplet-matrix morphology it decreases the absolute value of $\langle H\rangle$.

The local shape of the interface can be studied by constructing curvature probability distribution functions [9,28]. In Fig. 11, the local mean curvature probability distributions are shown for all six models considered in this paper. Only for the unmodified homogeneous Landau-Ginzburg free energy [Eq. (19)] is a considerable change of the $P(H)$ shape observed. This suggests that neither the concentration dependence of the Onsager coefficient non the concentration dependence of the square gradient coefficient significantly affects local properties of the interface.

III. CONCLUSIONS

The spinodal decomposition of the homopolymer blend has been simulated within several mesoscopic models. The influence of the three following factors have been investigateds: the form of the homogeneous part of the free-energy

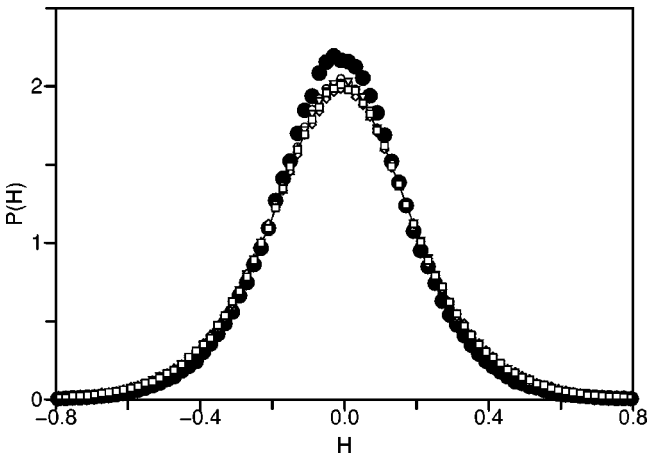

FIG. 11. The local mean curvature probability distribution functions calculated for the phase separated morphology after 390 rescaled time units of the simulated spinodal decomposition for different models. The symbols corresponds to the considered model as follows: the nonmodified LG (filled circles), modified LG ($\diamond$), and FH (∇) homogeneous free energies with constant Onsager and square-gradient coefficients; the FHD (squares) and FHL ($\bigcirc$) free energies with concentration dependent Onsager coefficients; and the FH homogeneous free energy, and constant Onsager and concentration dependent square-gradient coefficients ($\triangle$). The quench condition is $\phi_0=0.5$ at $T=25\,^{\circ}\mathrm{C}$.

functional, the concentration dependence of the square gradient coefficient, and the concentration dependence of the Onsager coefficient.

In the case of symmetric blends the most important factor that quantitatively determines the morphology development is the square-gradient coefficient in the free-energy functional K. From the dimension analysis one can extract the following time dependence for the characteristic length [3]: $L(t)\sim(\tilde{\sigma}t)^{1/3}$. For a flat interface, the interface tension $\tilde{\sigma}$ can be expressed as [1]

$$\tilde{\sigma}=K\int\left(\frac{dc}{dx}\right)^2 dx, \tag{26}$$

where the integration of the concentration profile $c(x)$ is performed in the direction normal to the interface. In the computer simulations the asymptotic exponent 1/3 for the average domain growth has never been achieved within the time interval studied. However, a qualitatively similar dependence of the growth laws on K has been observed. Due to the symmetry of the equilibrium phase volume fraction the growth law is not affected by the form of the equilibrium free energy; the average mean curvature of the interface remains zero. From a geometrical consideration, the product of the average domain size and the interface area density (S/V) must be a constant. Further, if one assumes that the dynamic scaling hypothesis also holds for the interface shape, then the average Gaussian curvature would scale as $K_G\sim L(t)^{-2}$. The change of the interface topology described by the Euler characteristic density can be found from the Gauss-Bonnet theorem: $\chi_{Euler}/V\sim L(t)^{-3}$. Therefore, more interconnected interfaces are observed for models with smaller square gradient coefficients [Fig. 7(b)]. Nevertheless, the concentration dependence of the square-gradient coefficient attributed to the Flory-Huggins–de Gennes free-energy functional has no significant influence on the average domain growth law and, consequently, on the interface topology [Figs. 2(c), 2(d), and Fig. 5(a)].

In the case of asymmetric blends ($\phi_0\neq 0.5$) the average domain growth is also governed by the surface tension, similarly to the symmetric blends. However, the interface topology in this case is also affected by one additional factor—the temporal evolution of the phase volume fraction. It was shown [9,26] that a transition from bicontinuous to droplet morphology occurs when the minority phase volume fraction becomes smaller than the percolation threshold value $f_{th}=0.3$. Therefore, the form of the equilibrium free energy that determines the final, equilibrium phase volume fractions has a crucial effect on the morphological development in the asymmetric blends (Fig. 3). The concentration dependence of the square-gradient coefficient does not change the equilibrium phase volume fractions, but it modifies the way the volume fractions approach their equilibrium values [Fig. 6(a)]. For all quench conditions studied here this fact does not modify the Euler characteristic density evolution. The average mean curvature is more sensitive to the phase volume fraction evolution [Fig. 4(b)]. In the case of bicontinuous asymmetric blends ($f_m^{eq}>0.3$), the transformation of the percolated cluster morphology into the interconnected passage structure (defined at $\langle H\rangle=0$) takes place more rapidly for a model with the concentration dependent square-gradient coefficient. In the case of disperse morphology, the concentration dependence of K results in smaller values of $\langle H\rangle$.

The influence of the square-gradient coefficient magnitude on the morphology development in asymmetric blends is more complex. A smaller square-gradient coefficient corresponds to a smaller surface tension $\tilde{\sigma}$ that, similarly to symmetric cases, modifies the scaling factor in the growth law: the domains have a smaller average size. However, it also changes the temporal evolution of the phase volume fractions [Fig. 7(d)]. For bicontinuous blends those minority volume fractions are larger than the percolation threshold; the interface shapes characterized by the dimensionless homogeneity indices are remarkably insensitive to the magnitude of K [Fig. 7(c)]. Nevertheless, for more asymmetric or shallow quenches, the time for the bicontinuous morphology transformation into a droplet-matrix structure depends strongly on K. The percolation threshold $f_{th}=0.3$ for the FHD model has been determined phenomenologically, by analyzing the available data. A similar analysis of the obtained results suggests that, in general, the value of the percolation threshold is model dependent: for a smaller K a smaller percolation threshold is observed.

The experimental verification of the model assumptions about the free-energy form can be made by measuring the maximum wave vector in the scattering intensity as a function of the minority phase volume fraction during the spinodal decomposition of the bicontinuous, asymmetric blends (Fig. 8). By comparing the experimental results with the simulation curves a definitive statement about concentration dependence of the square gradient coefficient and its magnitude can be made.

The concentration dependence of the Onsager coefficient has a weak, systematic effect on the morphology develop-

ment: it slows down the phase separation process (Figs. 9 and 10). Its relative magnitude for the change of the average domain size has been found smaller than 10% within the time interval studied. The local shape of the interface characterized by the local curvature probability distributions is not affected considerably by the concentration dependence of the square gradient and the Onsager coefficient (Fig. 11).

The results presented above suggest that despite highly nonlinear character of the Cahn-Hilliard-Cook equation, there are more simple relations between the characteristic morphological measures such as the Euler characteristic, average mean curvature, phase volume fraction and average domain size. A semiempirical model that allows one to reconstruct the three-dimensional morphology of the phase-separated blend without numerical integration of the Cahn-Hilliard-Cook equation is now being developed.

ACKNOWLEDGMENTS

R.H. was supported by KBN Grant No 2P03B12516. He also acknowledged the hospitality of ENS-Lyon and the stipend from the French Ministry of Education.

[1] J.S. Langer, in *Solids far from Equilibrium*, edited by C. Godrèche (Cambridge University Press, Cambridge 1992).
[2] J.D. Gunton, M. San Miguel, and P. S. Sahni, in *Phase Transition and Critical Phenomena*, edited by C. Domb and J. L. Lebowitz (Academic Press, London 1983), Vol. 8, pp. 267–455.
[3] A.J. Bray, Adv. Phys. **43**, 357 (1994).
[4] T.M. Rogers, K.R. Elder, and R.C. Desai, Phys. Rev. B **37**, 9638 (1988).
[5] A. Chakrabarti, R. Toral, J.D. Gunton, and M. Muthukumar, J. Chem. Phys. **92**, 6899 (1990).
[6] G. Brown and A. Chakrabarti, J. Chem. Phys. **98**, 2451 (1993).
[7] M.A. Kotnis and M. Muthukumar, Macromolecules **25**, 1716 (1992).
[8] H. Zhang, J. Zhang, and Y. Yang, Macromol. Theory Simul. **4**, 1001 (1995).
[9] A. Aksimentiev, K. Moorthi, and R. Hołyst, J. Chem. Phys. **112**, 6049 (2000).
[10] P. Pincus, J. Chem. Phys. **75**, 1996 (1981).
[11] E. Siggia, Phys. Rev. A **20**, 595 (1979).
[12] T. Koga and K. Kawasaki, Physica A **196**, 389 (1993).
[13] P.G. de Gennes, J. Chem. Phys. **72**, 4756 (1980).
[14] K. Binder, J. Chem. Phys. **79**, 6387 (1983).
[15] P. de Gennes, *Scaling Concepts in Polymer Physics* (Cornell University Press, Ithaca, NY, 1979).
[16] P. Wiltzius, F.S. Bates, and W.R. Heffner, Phys. Rev. Lett. **60**, 1538 (1988).
[17] H. Tang and K.F. Freed, J. Chem. Phys. **94**, 1572 (1991).
[18] A.Z. Akcasu and I.C. Sanchez, J. Chem. Phys. **88**, 7847 (1988).
[19] Y. Oono and S. Puri, Phys. Rev. Lett. **58**, 836 (1987).
[20] F.S. Bates, G.D. Wignall, and W.C. Koehler, Phys. Rev. Lett. **55**, 2425 (1985).
[21] W.T. Góźdź and R. Hołyst, Phys. Rev. E **54**, 5012 (1996); Phys. Rev. Lett. **76**, 2726 (1996).
[22] K.R. Mecke, Int. J. Mod. Phys. B **12**, 861 (1998).
[23] R. Hołyst, Curr. Opin. Colloid Interface Sci. **3**, 422 (1998).
[24] I. Szleifer and B. Widom, J. Chem. Phys. **90**, 7524 (1989).
[25] Y. Nishikawa, H. Jinnai, T. Koga, T. Hashimoto, and S.T. Hyde, Langmuir **14**, 1242 (1998).
[26] A. Aksimentiev, R. Hołyst, and K. Moorthi, Macromol. Theory Simul. (to be published).
[27] H. Jinnai, T. Koga, Y. Nishikawa, T. Hashimoto, and S.T. Hyde, Phys. Rev. Lett. **78**, 2248 (1997).
[28] H. Jinnai, Y. Nishikawa, and T. Hashimoto, Phys. Rev. E **59**, 2554 (1999).
[29] Z.H. Liu, X.P. Zhang, X.G. Zhu, Z.N. Qi, and F.S. Wang, Polymer **38**, 5267 (1997).
[30] S. Puri and Y. Oono, Phys. Rev. A **38**, 1542 (1988).